Exploring the initial errors that cause a significant "spring predictability barrier" for El Niño events

Wansuo Duan,[1] Xinchao Liu,[2] Keyun Zhu,[2] and Mu Mu[1]

Received 20 May 2008; revised 23 December 2008; accepted 27 January 2009; published 30 April 2009.

[1] Within the Zebiak-Cane model, we identify two types of initial errors that have significant season-dependent evolutions related to the spring predictability barrier (SPB) for El Niño events. One type includes the sea surface temperature anomaly (SSTA) errors that have a zonal dipolar pattern with positive anomalies in the central equatorial Pacific and negative ones in the eastern equatorial Pacific; the other type consists of the SSTA errors with a spatial structure opposite to that of the former type, the zonal dipolar pattern shows negative anomalies in the central equatorial Pacific and positive anomalies in the eastern equatorial Pacific. The patterns of these two types of errors are nearly opposite of each other. The former causes the El Niño event to be underpredicted, and the latter causes the El Niño event to be overpredicted. For strong El Niño events the former tends to have a larger effect on the predictions than the latter, but for weak El Niño events, it is very difficult to determine which type of initial errors results in worse predictions. It is thought that strong (weak) El Niño events could be affected by strong (weak) nonlinearities. There are also other initial errors; however, they do not yield considerable season-dependent evolutions nor can a common characteristic be extracted from their patterns. The two types of initial errors suggest two dynamical behaviors of error growth related to the SPB: in one case, the initial errors grow in a manner similar to the El Niño events; in the other case, the initial errors develop with a tendency opposite to the El Niño events. The two types of initial errors may capture the errors that exhibit significant season-dependent evolutions related to the SPB. In addition, they may provide information regarding the "sensitive area" of ENSO predictions because of their localized regions. Therefore, if these types of initial errors exist in the realistic El Niño–Southern Oscillation (ENSO) predictions and if a data assimilation or a target method can filter them, the ENSO forecast skill may be improved. For ensemble forecast studies, different signs of prediction errors caused by the two types of initial errors could illustrate why the ensemble mean offers a better forecast than a single prediction.

Citation: Duan, W., X. Liu, K. Zhu, and M. Mu (2009), Exploring the initial errors that cause a significant ''spring predictability barrier'' for El Niño events, *J. Geophys. Res.*, *114*, C04022, doi:10.1029/2008JC004925.

1. Introduction

[2] El Niño–Southern Oscillation (ENSO), a prominent climate phenomenon in the coupled ocean-atmosphere system of the tropical Pacific, has a great impact on the global climate. In the past three decades, the ENSO has received tremendous attention. While significant progress has been made in ENSO theories and predictions over the years, especially through the TOGA (Tropical Ocean Global Atmosphere) program (see the review of *Wang and Picaut* [2004]), there still exist considerable uncertainties in realistic ENSO predictions [*Jin et al.*, 2008]. In particular, if forecasts are made before and through the spring, ENSO predictions tend to be much less successful. This low predictability has been related to the so-called "spring predictability barrier" (SPB) of the ENSO.

[3] The SPB is a well-known characteristic of ENSO forecasts [*Webster and Yang*, 1992; *Lau and Yang*, 1996; *McPhaden*, 2003], which refers to the phenomenon that most ENSO prediction models often experience an apparent drop in prediction skill across April and May [*Latif et al.*, 1994]. SPBs exist in coupled and statistical models. In some cases, the SPB is even stronger in statistical models than in general circulation models (GCMs) [*van Oldenborgh et al.*, 2005]. Considerable efforts have been made in studying this phenomenon [e.g., *Walker*, 1924; *Moore and Kleeman*, 1996; *Samelson and Tziperman*, 2001; *McPhaden*, 2003], but its cause remains controversial. One of the possible causes is the rapid seasonal transition of monsoon circulation during the boreal spring, which perturbs the Pacific basic state when the east-west sea surface temperature (SST) gradient is the

[1] LASG, Institute of Atmospheric Physics, Chinese Academy of Sciences, Beijing, China.
[2] Department of Atmospheric Science, Chengdu University of Information Technology, Chengdu, China.

0148-0227/09/2008JC004925

weakest [*Webster and Yang*, 1992; *Lau and Yang*, 1996]. Another notion proposed by *Webster* [1995] is that the SPB is due to the weakest ocean-atmosphere coupling occurring during the spring in the eastern Pacific. Other studies argued that the SST anomalies in the boreal spring are relatively small, such that these anomalies are difficult to detect and forecast in the presence of atmospheric and oceanic noises [*Chen et al.*, 1995; *Xue et al.*, 1997]. *Samelson and Tziperman* [2001] demonstrated that the SPB is an inherent characteristic of the ENSO, whereas *Chen et al.* [2004] suggested that this predictability barrier could be reduced through improving initialization. *McPhaden* [2003] showed that subsurface information has a winter persistence barrier and that the predictability of the ENSO across the spring may potentially be enhanced by incorporating this information into the model. In general, the cause of the SPB remains elusive. There is an urgent need to further address the problems related to the SPB for the ENSO.

[4] A number of papers have emphasized the role of initial errors in the SPB. *Moore and Kleeman* [1996] investigated the season-dependent evolutions of initial errors related to the SPB. *Chen et al.* [1995] eliminated the SPB phenomenon of the model developed by *Zebiak and Cane* [1987] through improving initialization. Recently, *Mu et al.* [2007a, 2007b] demonstrated that the SPB may be a result of the combined effect of three factors: the climatological annual cycle, the El Niño event itself, and the initial error pattern. The former two factors remain in the model and are the origin of the seasonality of error growth. It has been suggested that, even if the seasonality of error growth is determined by the model, particular initial error modes are necessary to bring about the SPB [*Mu et al.*, 2007a]. That is, there exists the possibility that some types of initial errors may cause extreme uncertainties in ENSO forecasting through the spring and exhibit a prominent season-dependent evolution related to the SPB, because of the seasonality of ocean-atmosphere coupling, while other types tend to yield an unapparent season-dependent evolution. The initial errors could play an important role in the occurrence of the SPB for the ENSO. *Mu et al.* [2007b] used the Zebiak-Cane model [*Zebiak and Cane*, 1987] to investigate the initial error that causes a significant SPB by computing the conditional nonlinear optimal perturbation (CNOP) [*Mu et al.*, 2003] for El Niño events and argued that the CNOP-type error cause a notable SPB. However, the CNOPs are not generally computed in realistic ENSO predictions. Thus, some questions need to be addressed: do there exist initial errors similar to CNOPs in ENSO predictions? what features display initial error patterns that exhibit a significant season-dependent evolution related to the SPB for ENSO events?

[5] In this paper, we will explore these questions by performing perfect model predictability experiments with the Zebiak-Cane model. The so-called perfect predictability experiments means that the numerical models are assumed to be perfect in predictability experiments and one only considers the effect of initial errors on the prediction uncertainties. In fact, this belongs to the studies of the first kind of predictability proposed by *Lorenz* [1975]. In this paper, to explore the characteristic of initial errors that exhibit a significant season-dependent evolution related to the SPB for El Niño events, a large number of El Niño events are chosen from a time series of SST anomalies (SSTA) in the Zebiak-Cane model. These El Niño events are predicted with the perturbed initial fields and the seasonal growth rates of the initial uncertainties are estimated. For the initial errors that have prominent season-dependent growth related to the SPB, we evaluate their pattern structures in attempt to determine common characteristic among them.

[6] The paper is organized as follows. In section 2, the Zebiak-Cane model is described. The main results are reported in section 3. In section 4, we discuss the implications of the results. Finally, a conclusion and a discussion are presented in section 5.

2. ENSO Model

[7] The Zebiak-Cane model was the first coupled ocean-atmosphere model to simulate the interannual variability of the observed ENSO and has been a benchmark in the ENSO community for over two decades. The Zebiak-Cane model has been widely used in predictability studies and predictions of the ENSO [*Zebiak and Cane*, 1987; *Blumenthal*, 1991; *Xue et al.*, 1994; *Chen et al.*, 2004; *Tang et al.*, 2008]. It is composed of a Gill-type steady state linear atmospheric model and a reduced-gravity oceanic model, which depict the thermodynamic and atmospheric dynamics in the tropical Pacific with oceanic and atmospheric anomalies about the mean climatological state specified from observations [see *Zebiak and Cane*, 1987].

[8] The atmospheric dynamics is described by the steady state linear shallow water equations on an equatorial beta plane. The circulation is forced by a heating anomaly that depends partly on local heating associated with SST anomalies and partly on low-level moisture convergence (parameterized in terms of the surface wind convergence [*Zebiak*, 1986]). Here, the convergence feedback is a nonlinear process because the moisture-related heating is operative only when the total wind field is convergent, and this depends not only on the calculated convergence anomaly, but also on the specified mean convergence. The important effect of the feedback is to focus the atmospheric response to the SST anomalies into or near the regions of mean convergence, in particular, the Intertropical Convergence Zone and the Southern Pacific Convergence Zone.

[9] The thermodynamics are governed by an evolution equation of the SSTA in the tropical Pacific that includes three-dimensional temperature advection by both the specified mean currents and the calculated anomalous currents. The assumed surface heat flux anomaly is proportional to the local SST anomaly, always acting to adjust the temperature field toward its climatological mean state, which is specified from observation.

[10] In the model run, the atmosphere is previously run with the specified monthly mean SST anomalies to simulate monthly mean wind anomalies. Then the ocean component is forced by surface wind stress anomalies that are generated from a combination of the surface wind anomalies produced by the atmosphere model and the background mean winds.

3. Results

3.1. Experimental Strategy

[11] In perfect model predictability experiments, the model ENSO events, which are obtained by integrating the model

with proper initial conditions, could be predicted with perturbed initial fields [*Smith et al.*, 1999; *Mu et al.*, 2007a, 2007b]. On the basis of this viewpoint, *Xu and Duan* [2008] estimated the predictability of the Zebiak-Cane model by predicting the maximum prediction errors of model ENSO events. Their results indicated that the ENSO warming event is rarely predictable through the spring, mimicking the behavior of the SPB. In this paper, we will investigate the characteristic of the initial errors that cause a significant SPB for model El Niño events.

[12] By integrating the Zebiak-Cane model for 1000 model years, we obtained a time series of NINO3 SSTA (averaged SSTA in the east Pacific 150°W-90°W, 5°S-5°N). In this series, there are many El Niño events with different intensities, which have a dominant period of 4 years [*Pan et al.*, 2005]. Furthermore, with the present model parameters, most of the model El Niño events tend to warm initially during January–April or September–November, that is, they prefer to transit from cold to warm during January–April or September–November (Figure 1). In this study, the El Niño events to be predicted are therefore considered to be two types of model El Niño events: events with initial warming in January–April, and events with initial warming in September–November.

[13] In the numerical experiments, the 1000 model years are divided into ten continuous time intervals starting with year 0–99, year 100–199, and so on. In each of these ten time intervals, two strong and two weak El Niño events are respectively chosen, where the strong (weak) El Niño events refer to events in which the NINO3 SSTA are larger (less) than 2°C in the Zebiak-Cane model. A total of 40 El Niño events are obtained, including 12 events with initial warming in January–April and 28 events with initial warming in September–November. All these El Niño events are predicted through the spring with the start month being their initial warming time plus a leading time of 12 months.

[14] The initial uncertainties in this study are superimposed on the SSTA and thermocline depth anomaly fields of the "true state" El Niño events. Although the atmosphere is previously perturbed in the coupled models, in the Zebiak-Cane model, it is described by the steady state linear shallow water equation (see section 2), in which the variations of the atmospheric perturbations are controlled by time-dependent oceanic variables such as SSTA, thermocline depth anomalies, etc. Therefore, we perturb the components of SSTA and thermocline depth anomaly in the perfect predictability experiments of this study, where the initial uncertainties are taken from the time series of the model SSTA and thermocline depth anomalies. The model ENSO has a dominant period of about 4 years. For the dimensional SSTA and thermocline depth anomaly patterns in each month of the 4 years preceding each El Niño year, we scale them to yield the initial uncertainties. Thus, we have 48 different initial error patterns to add on the initial values of each El Niño event. Each of these initial error patterns is analyzed. The details are as follows. We denote the dimensional SSTA and thermocline depth anomalies as T with grid points T_{ij} and h with h_{ij}, where (i, j) represents the grid points in the region with latitude ranging from 129.375E to 84.375W by 5.625 and longitude from 19S to 19N by 2. T and h are then scaled by $T_0 = T/\delta$ and $h_0 = h/\delta$ with an appropriate fraction $1/\delta$ (δ is a positive number), respectively. T_0 and h_0 are then regarded as the initial errors superimposed onto the initial states of the El Niño events in the following theoretical prediction experiments.

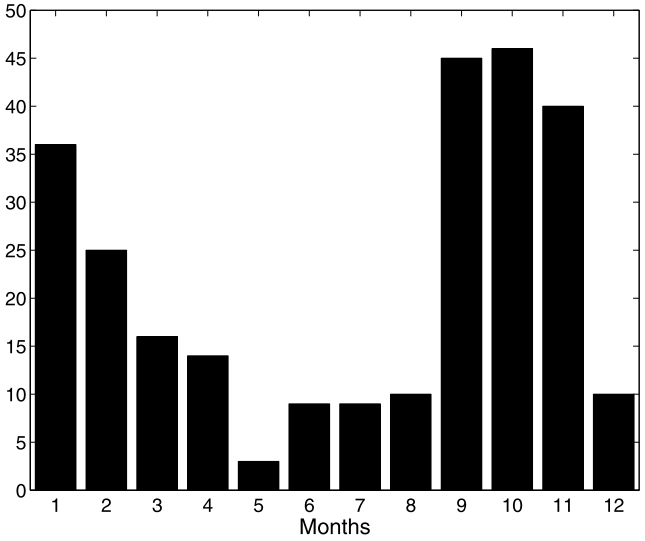

Figure 1. A histogram of the number of ENSO events with initial warming in each month of the calendar year. The horizontal axis indicates the months of the calendar year, and the vertical axis denotes the number of ENSO events with initial warming in each month.

[15] To measure the magnitudes of the initial errors, the characteristic scales of the SST and thermocline depth, $w_1 = 2°C$ and $w_2 = 50$ m are used to non-dimensionlize the initial errors T_0 and h_0 [*Wang and Fang*, 1996]. We have $T_0' = \frac{T_0}{w_1}$ and $h_0' = \frac{h_0}{w_2}$. Then, T_0' and h_0' respectively represent the nondimensional initial errors of SSTA and thermocline depth anomaly components for the "true state" El Niño events. The norms $\|T_0'\| = \sqrt{\Sigma_{i,j}\left(T_{0ij}'\right)^2}$ and $\|h_0'\| = \sqrt{\Sigma_{i,j}\left(h_{0ij}'\right)^2}$ are used to constrain the magnitudes of the initial errors, i.e., $\|T_0'\| = \|h_0'\| = \sigma$. By adjusting the value of σ, different magnitudes of initial errors can be obtained.

[16] For each of the 40 chosen El Niño events, we integrate the Zebiak-Cane model for 12 months with its own 48 different perturbed initial conditions and obtain the 48 predictions of the Niño-3 indices for each El Niño event. The difference between the "true states" and their predictions is generally referred to as prediction error. In prefect model predictability experiments, the prediction error is only caused by the growth of initial errors. In this paper, we will explore the dynamical behaviors of these prediction errors (i.e., the evolutions of initial errors) at different seasons and investigate the common characteristic of the initial errors that exhibit significant season-dependent evolutions related to the SPB for El Niño events. A calendar year is divided into four "seasons" starting with January–March (JFM), followed by April–June (AMJ), and so forth. Since NINO3 SSTA are generally used to determining whether an El Niño event is occurring, the slope κ of the curve $\gamma(t) = \|T'(t)\|$ related to the NINO3 SSTA is computed at different seasons, where $T'(t)$ is the difference between the predicted SSTA in Nino-3 region and those of the "true state" El Niño events and acts as the prediction errors of El Niño events

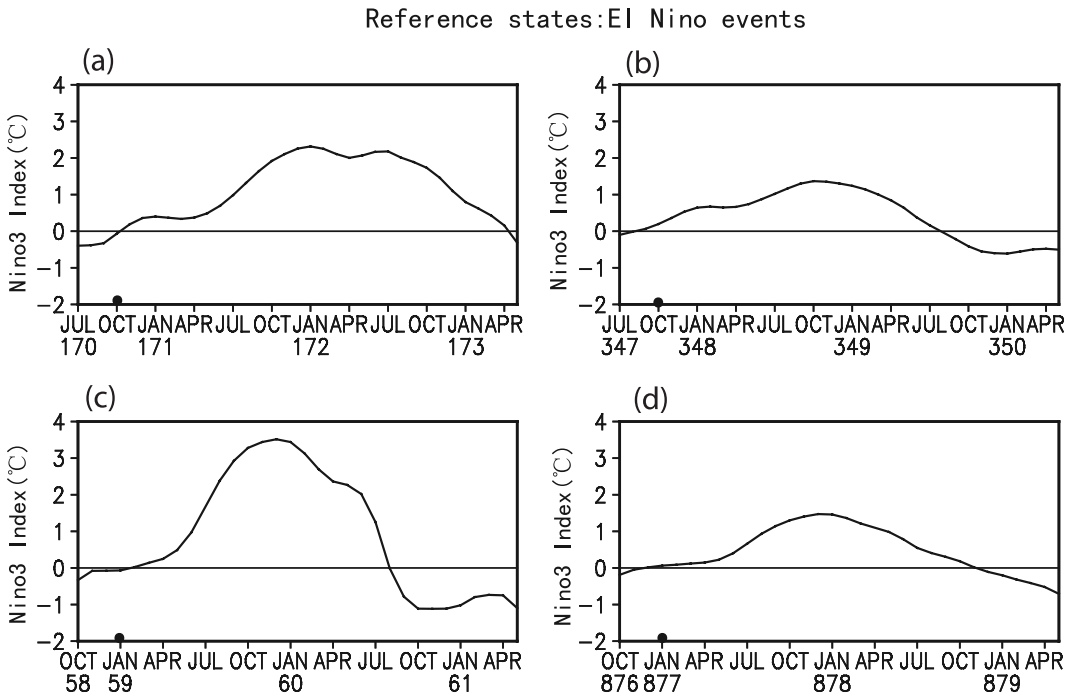

Figure 2. Four examples of the chosen El Niño events: (a) strong event and (b) weak event with initial warming in October and (c) strong event and (d) weak event with initial warming in January.

caused by initial errors (T_0', h_0'). The slope κ describes the tendency of seasonal growth for SSTA component of initial errors. The prediction error, $T'(t)$ here is measured by the norm $\|T'(t)\| = \sqrt{\Sigma_{i,j}\left(T(t)'_{ij}\right)^2}$, where (i,j) represents the grid points in the Nino-3 region. A positive (negative) value of κ corresponds to an increase (decrease) in the SSTA errors, and the larger the absolute value of κ, the faster the increase (decrease).

3.2. Tendencies of Initial Error Growth at Different Seasons

[17] For each of the chosen 40 El Niño events, the corresponding 48 initial error patterns are superimposed on it to investigate the slope, κ of the error growth related to the SPB. For each initial error superimposed onto an El Niño event, there are four seasonal slopes κ to be calculated. Denoting the largest positive slope as $\kappa_{\max}$ and the second largest positive slope as $\kappa_{\text{s-max}}$, we can use these two factors to explore the season during which the initial error growth is significantly larger than those at other seasons. In this section, we prescribe that if $\kappa_{\max} > 1$ and $\kappa_{\max} - \kappa_{\text{s-max}} > 0.5$ [*Mu et al.*, 2007a, 2007b], the error growth at the season corresponding to $\kappa_{\max}$ is considerably larger than those at other seasons. Here, $\kappa_{\max} > 1$ indicates that the prediction error measured by the chosen norm is amplified exceeding 1 (nondimensional; dimensional 2°C) at the corresponding season; $\kappa_{\max} - \kappa_{\text{s-max}} > 0.5$ means that the magnitude of the prediction error growth at the season of $\kappa_{\max}$ is 0.5 (nondimensional; dimensional 1°C) larger than that at the season of $\kappa_{\text{s-max}}$.

[18] Within the above approach, we study the seasonal evolutions of different initial error patterns on model El Niño events. In the numerical experiments, the El Niño events are predicted through spring with the start month being their initial warming times. For example, in the case of the El Niño event shown in Figure 2a, the initial warming occurs in October, so the prediction is carried out with October as the start month. In addition, for the initial error constraints, we tried several reasonable values of σ ranging from 0.5 to 1.2. Similar results are obtained for the chosen 40 El Niño events. For simplicity, we take only $\sigma = 0.8$, i.e., $\|T'\| = \|h'\| = 0.8$, to show our results.

[19] We first consider the El Niño events with initial warming in September–November. This type of El Niño events tend to peak at the end of next year. In the predictability experiments, there are 28 such El Niño events to be considered (see section 3.1). By investigating the initial errors of these El Niño events, we find that, although the error patterns that exhibit significant season-dependent evolutions have common characteristics, their effects on El Niño predictions show some differences between strong and weak El Niño events. Therefore, we will describe the results of the strong and weak El Niño events.

[20] For the strong El Niño events with initial warming in September–November, the slopes κ of each of the 48 different initial errors with $\sigma = 0.8$ are calculated to evaluate the seasonal tendencies of the error growths. It is found that for each of these strong El Niño events, some of its own 48 initial error patterns yield extreme uncertainties in the El Niño predictions, in which most initial errors tend to grow considerably during the AMJ season and exhibit prominent season-dependent evolutions, while a few initial errors have significant growth in AMJ and JAS, with the largest growth rates occurring in JAS. As an example of these strong El Niño events (see Figure 2a), we illustrate in Table 1 eight cases of the initial errors that yield extreme prediction uncertainties, of which seven have the largest growth occurring in AMJ, and one has significant growth in AMJ and JAS

Table 1. Seasonal Growth Rates of Types I and II Errors for the Strong El Niño With Initial Warm in October[a]

SSTA Errors	OND	JFM	AMJ	JAS	$E_{Nino\text{-}3}$
Error 11	0.312	1.695	**5.833**	4.657	−1.294
Error 12	0.521	1.971	**5.819**	4.611	−1.322
Error 13	0.622	1.848	**4.269**	**5.743**	−1.299
Error 14	0.195	1.651	**6.170**	4.913	−1.334
Error 21	0.093	0.977	**2.891**	1.517	0.561
Error 22	0.114	1.116	**2.551**	1.363	0.528
Error 23	0.183	1.146	**2.923**	1.647	0.594
Error 24	−0.060	0.739	**3.173**	2.052	0.612

[a]Bold denotes seasons when the error growth is considerable.

with the largest occurring in JAS. $E_{Nino\text{-}3}$ there represents the uncertainties of the El Niño predictions with 1 year lead time, which are caused by the corresponding initial errors and obtained by subtracting the NINO3 SSTA of the "true state" from that of the predicted state. The negative (positive) values of $E_{Nino\text{-}3}$ indicate an under-prediction (over-prediction) of the event. The numerical results demonstrate that the initial errors that exhibit prominent season-dependent evolutions for the strong El Niño events with initial warm in September–November can be classified into two types: those that result in negative errors in the NINO3 SSTA for El Niño events (i.e., the negative values of $E_{Nino\text{-}3}$) and cause an under-prediction of El Niño events and those that induce positive prediction errors of El Niño events (i.e., the positive values of $E_{Nino\text{-}3}$) and cause an over-prediction of El Niño events. The eight initial errors listed in Table 1 are examples of such errors (see the column of "$E_{Nino\text{-}3}$"). There also exist other initial errors in strong El Niño events that do not show considerable season-dependent evolutions, although they have the same magnitudes as the above two types of initial errors. Table 2 lists the seasonal growth rates (i.e., the slope κ) of some of such initial errors for the El Niño event shown in Figure 2a.

[21] Figure 3a (3b) shows the SSTA components of the eight initial errors listed in Table 1, which shows that the SSTA components of the initial errors that cause the El Niño to be under-predicted may have a common characteristic of possessing a large-scale zonal dipolar pattern with positive anomalies in the central equatorial Pacific and negative anomalies in the eastern equatorial Pacific (Figure 3a; hereafter referred to as Type I errors), but the initial errors that cause the El Niño to be over-predicted have a SSTA component with a zonal dipolar pattern with negative anomalies in the central equatorial Pacific and positive anomalies in the eastern equatorial Pacific (Figure 3b; hereafter referred to as Type II errors). This common characteristic of the eight initial errors listed in Table 1 led us to investigate whether all such initial errors possess a large-scale dipolar structure of SSTA components for all the strong El Niño events with initial warming in September–November. To address this, we took the composite of the initial errors that cause those strong El Niño events to be under-predicted and to be over-predicted, respectively (Figure 4). It is shown that the composite SSTA component also tends to exhibit the large-scale dipolar patterns shown in Figures 3a and 3b, which indicates that the large-scale dipolar pattern of SSTA component could be the dominating characteristic of initial errors that exhibit significant season-dependent evolutions for strong El Niño events. In addition, we also find that for the strong El Niño events, although both types of initial errors have significant season-dependent evolutions, the Type-I errors tend to have a greater effects on the predictions, because of their larger resultant prediction errors in the NINO3 SSTA (see Table 1 and section 4). For the error patterns without an apparent seasonal evolution, we find that it is very difficult to identify a common characteristic among them. In Figure 3c, we plot the SSTA component of four examples of such errors listed in Table 2.

[22] For the thermocline components of the Type-I errors (Type-II errors), we note that the evolution behaviors are favorable for Type-I errors (Type-II errors) yielding negative (positive) prediction errors in the NINO3 SSTA for El Niño events and making the predicted El Niño events weaker (stronger). This indicates that the thermocline depth components cause the Type-I errors (Type-II errors) to evolve into La Niña–like (El Niño–like) events because of the Bjerknes' positive feedback mechanism (for details, see section 4).

[23] For the weak El Niño events with initial warming in September–November, we also explored the characteristics of the initial errors that have significant growth during the spring. The results demonstrate that there exist two types of initial errors, which have patterns similar to that of Type-I and Type-II errors and exhibit significant season-dependent evolutions. Table 3 lists the seasonal growth rates of some of these two types of initial errors for the weak El Niño event in Figure 2b. For convenience, we designate these two types of initial errors as Type-I and Type-II errors as well. Type-I errors cause the El Niño events to be under-predicted and Type-II errors cause the El Niño events to be over-predicted. Nevertheless, in the case of weak El Niño events, we cannot determine which type of error patterns have a larger effect on the predictions. For some weak El Niño events in the numerical experiments, Type-I errors yield larger prediction errors, while in other events, Type-II errors produce the larger prediction errors. Sometimes the prediction errors caused by these two types of initial errors exhibit only a trivial difference in amplitude. Likewise, it is also found that, in addition to these two types of initial errors, there exist other initial errors, which do not have an obvious season-dependent growth. Furthermore, we cannot extract a common characteristic from their patterns.

[24] The initial errors of the El Niño events with initial warming occurring in January–April were also investigated. In the numerical experiments, there are 12 such El Niño events to be studied. These El Niño events tend to peak at the end of year. Figures 2c and 2d show two examples of such El Niño events, including a strong and a weak event. For the 12 El Niño events, we investigate the initial errors that show significant season-dependent evolutions. It is shown that these initial errors tend to grow significantly in AMJ and JAS with maximum growth rate appearing in JAS, which is

Table 2. Seasonal Growth Rates of Other Type of Errors for the Strong El Niño With Initial Warm in October

SSTA Errors	OND	JFM	AMJ	JAS	$E_{Nino\text{-}3}$
Error 1	−0.879	−0.061	0.350	0.309	−0.105
Error 2	−0.762	−0.358	−0.146	0.519	0.083
Error 3	−0.830	−0.001	−0.020	0.214	−0.057
Error 4	−0.439	−0.069	−0.110	0.497	0.139

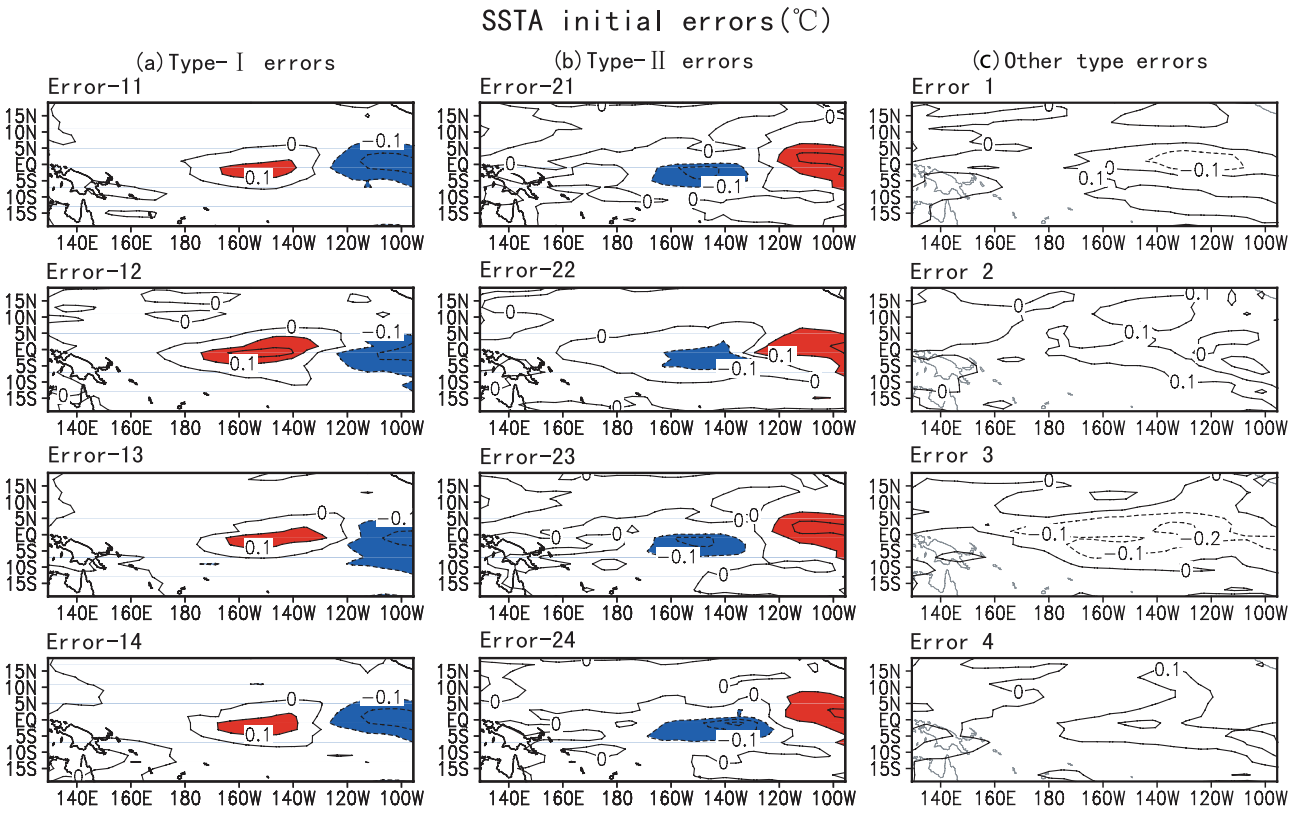

Figure 3. (a) Type I errors and (b) Type II errors: examples of two types of initial errors that have significant season-dependent evolutions related to the SPB for the strong El Niño event shown in Figure 2a. (c) Examples of the initial errors that do not have obvious season-dependent growth for the strong El Niño event shown in Figure 2a.

slightly different from those of the El Niño events with initial warming in September–November. Tables 4 and 5 list the seasonal growth rates of a few such initial errors for the El Niño events shown in Figures 2c and 2d, respectively. For this situation, *Mu et al.* [2007b] argued that although the maximum growth of the initial errors appears in JAS, the error growth during AMJ also becomes large, which may cause the dramatic decrease in El Niño forecast skill during AMJ. Despite this difference, the initial errors that show obvious season-dependent evolutions can still be classified into two types, such as those of the El Niño events with initial warming in September–November: errors that cause the El Niño to be under-predicted through the spring and errors that cause the El Niño to be over-predicted. The data in Tables 4 and 5 illustrate some of these two types of errors for the two examples El Niño events shown in Figures 2c and 2d. In addition, the patterns of these two types of initial errors (and their composite) are similar to those shown in Figures 3a and 3b (and Figure 4). That is, the former characterizes the SSTA component as a zonal dipolar pattern with positive anomalies in the central equatorial Pacific and negative anomalies in the eastern equatorial Pacific and the latter exhibits the SSTA component as a zonal dipolar pattern with negative anomalies in the central equatorial Pacific and positive anomalies in the eastern equatorial Pacific. For the strong El Niño events, the former error patterns tend to have a larger negative effect on the prediction than the latter ones. It is also shown that, for the initial errors that do not have obvious season-dependent evolutions, a common characteristic cannot be extracted from their patterns.

[25] The above analysis has identified two types of initial error patterns (for different El Niño events), Type-I and Type-II errors, that exhibit significant season-dependent evolutions and have a considerable effect on the predictions of El Niño events in the ZC model. To support this classification, we simply performed a cluster analysis experiment, in which the SSTA components of all the initial errors that exhibit significant season-dependent evolutions are collected as the objects (a total of 483 ones for the 40 El Niño events) for cluster analysis. A similarity coefficient is used to measure the similarity between the objects (SSTA components of initial errors). Let matrices $T_\alpha = (T^\alpha_{ij})_{m\times n}$ and $T_\beta = (T^\beta_{ij})_{m\times n}$ be two different SSTA error patterns, where T^α_{ij} and T^β_{ij} represent the values of initial errors at different grid points. We rewrite these two matrices into two column vectors

$$T'_\alpha = \{T^\alpha_{11}, T^\alpha_{12}, \cdots, T^\alpha_{1n}, T^\alpha_{21}, T^\alpha_{22}, \cdots, T^\alpha_{2m}, \cdots, T^\alpha_{m1}, T^\alpha_{m2} \cdots, T^\alpha_{mn}\}^\top,$$

$$T'_\beta = \{T^\beta_{11}, T^\beta_{12}, \cdots, T^\beta_{1n}, T^\beta_{21}, T^\beta_{22}, \cdots, T^\beta_{2m}, \cdots, T^\beta_{m1}, T^\beta_{m2}, \cdots, T^\beta_{mn}, \}^\top.$$

Then the similarity coefficient can be calculated by

$$\gamma = \cos\theta_{\alpha\beta} = \frac{T'^\top_\alpha \cdot T'_\beta}{\|T'_\alpha\|\|T'_\beta\|} = \frac{\Sigma^m_{i=1}\Sigma^n_{j=1} T^\alpha_{ij} T^\beta_{ij}}{\sqrt{\Sigma^m_{i=1}\Sigma^n_{j=1}\left(T^\alpha_{ij}\right)^2 \Sigma^m_{i=1}\Sigma^n_{j=1}\left(T^\beta_{ij}\right)^2}},$$

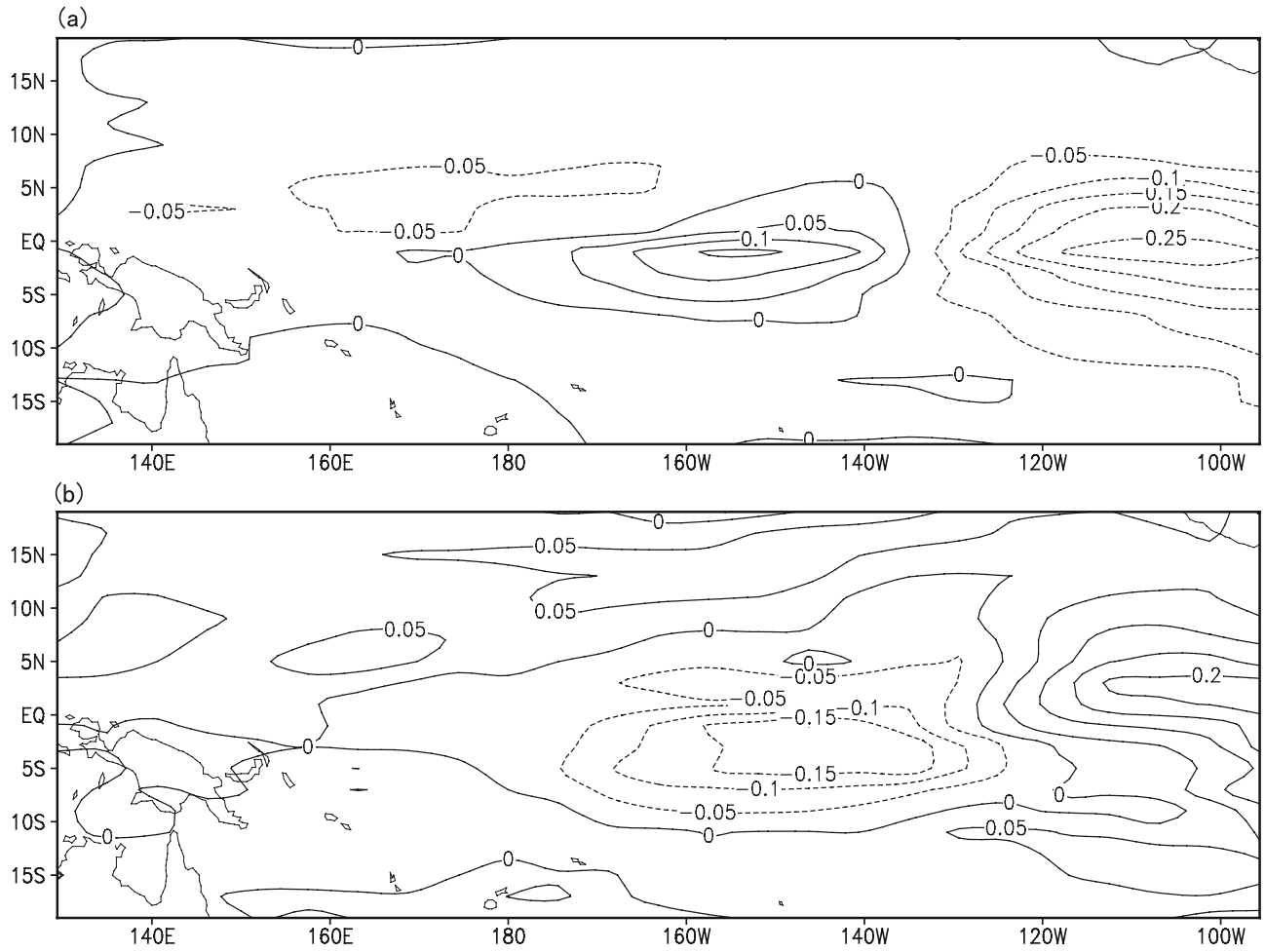

Figure 4. Composite of the initial errors (superimposed on the strong El Niño events with initial warming in September–November) that exhibit significant season-dependent evolutions: (a) composite of Type I errors and (b) composite of Type II errors.

where γ is the similarity coefficient and $\cos\theta_{\alpha\beta}$ represents the cosine of the angle between the two column vectors, T'_α and T'_β. By using the statistical software of SPSS (Statistical Product and Service Solutions), we classified the 483 initial errors into two groups: one consists of 263 initial errors, and the other has 220 ones. Then, we took the composite of the SSTA errors in each group and obtained two composite patterns (Figure 5). It is found that these two patterns are very similar to those in Figures 3 and 4, also exhibiting large-scale zonal dipolar patterns of SSTA components with positive anomalies in the equatorial central Pacific and negative anomalies in the equatorial eastern Pacific, and with negative anomalies in equatorial central Pacific and positive anomalies in equatorial eastern Pacific, respectively. It is therefore reasonable to suggest that the Type-I and Type-II errors may illustrate the dominant characteristic of initial errors that exhibit significant season-dependent evolutions for El Niño events.

4. Implications

[26] The results presented here have demonstrated that there exist two types of initial errors that show significant season-dependent evolutions, which are therefore related to

Table 3. Seasonal Growth Rates of Type I and II Errors for the Weak El Niño With Initial Warm in October[a]

SSTA Error	OND	JFM	AMJ	JAS	$E_{Nino\text{-}3}$
Error 11	0.020	0.964	**2.355**	0.975	−0.452
Error 12	0.389	1.234	**2.947**	0.764	−0.511
Error 13	−0.109	0.913	**2.856**	1.171	−0.477
Error 14	−0.058	0.899	**2.436**	1.046	−0.458
Error 21	−0.035	0.630	**2.898**	2.143	0.493
Error 22	−0.050	0.774	**2.503**	1.728	0.533
Error 23	−0.286	0.514	**2.317**	1.532	0.449
Error 24	−0.001	0.704	**2.929**	1.938	0.574

[a]Bold denotes seasons when the error growth is considerable.

Table 4. Seasonal Growth Rates of Type I and II Errors for the Strong El Niño With Initial Warm in January[a]

SSTA Errors	JFM	AMJ	JAS	OND	$E_{Nino\text{-}3}$
Error 11	0.246	**2.609**	**2.759**	−1.501	−0.306
Error 12	0.410	**3.437**	**3.936**	−1.167	−0.549
Error 13	0.109	**2.509**	**3.511**	−0.861	−0.428
Error 14	−0.177	**2.229**	**4.236**	−0.128	−0.561
Error 21	−0.072	**1.771**	**2.576**	−1.384	0.126
Error 22	0.098	**1.647**	**2.251**	−1.311	0.105
Error 23	−0.032	**1.857**	**2.424**	−1.398	0.115
Error 24	−0.219	**1.747**	**3.312**	−1.267	0.171

[a]Bold denotes seasons when the error growth is considerable.

Table 5. Seasonal Growth Rates of Type I and II Errors for the Weak El Niño With Initial Warm in January[a]

SSTA Errors	JFM	AMJ	JAS	OND	$E_{Nino\text{-}3}$
Error 11	0.472	**4.006**	**4.498**	−0.591	−0.860
Error 12	0.580	**4.691**	**4.680**	−1.613	−0.856
Error 13	0.305	**4.129**	**5.078**	−0.527	−0.905
Error 14	0.411	**4.029**	**4.614**	−0.634	−0.861
Error 21	0.078	**2.651**	**3.499**	0.569	0.719
Error 22	0.048	**2.911**	**4.975**	1.743	0.983
Error 23	−0.107	**2.501**	**4.208**	1.227	0.822
Error 24	0.087	**2.844**	**4.348**	1.206	0.872

[a]Bold denotes seasons when the error growth is considerable.

the SPB for El Niño events. There are Type-I-like errors that possess a SSTA component of a zonal dipolar pattern with positive anomalies in the central equatorial Pacific and negative anomalies in the eastern equatorial Pacific and yield negative prediction errors in the NINO3 SSTA for El Niño events; and there are Type-II-like errors that have a spacial pattern almost opposite to that of Type-I-like errors and cause positive prediction errors in the NINO3 SSTA. These results suggest that Type-II-like errors affect El Niño prediction by strengthening the El Niño amplitude and cause the predicted El Niño to be warmer. It is conceivable that Type-II-like errors may evolve into El Niño-like events, because of their particular signs, such that they could enhance the development of an El Niño event in the model. That is to say, Type-II-like errors could evolve into a positive NINO3 SSTA and have dynamical growth behavior similar to that of the "true state" El Niño. Since Type-I-like errors have the opposite sign, they could develop into a negative NINO3 SSTA, a La Niña–like event, which would decrease the amplitude of the El Niño event and make the predicted El Niño weaker, indicating that Type-I-like errors have a growth behavior opposite to that of the El Niño event. We have verified these points by examining the evolutions of the two composite errors (shown in Figure 5) on the 40 El Niño events. In Figures 6 and 7, we illustrate this result for two El Niño events: a strong El Niño event, i.e., the model 59/60 El Niño event shown in Figure 2c, and a weak event, the model 877/878 El Niño event shown in Figure 2d.

[27] The above two types of initial error patterns have dynamical growth behaviors similar to that of El Niño and La Niña events. It is known that the development of El Niño and La Niña events are now understood as a result of *Bjerknes'* [1969] positive feedback. We therefore infer that these two types of initial error patterns have the same growth mechanism as those of ENSO events and also result, in essence, from Bjerknes' positive feedback.

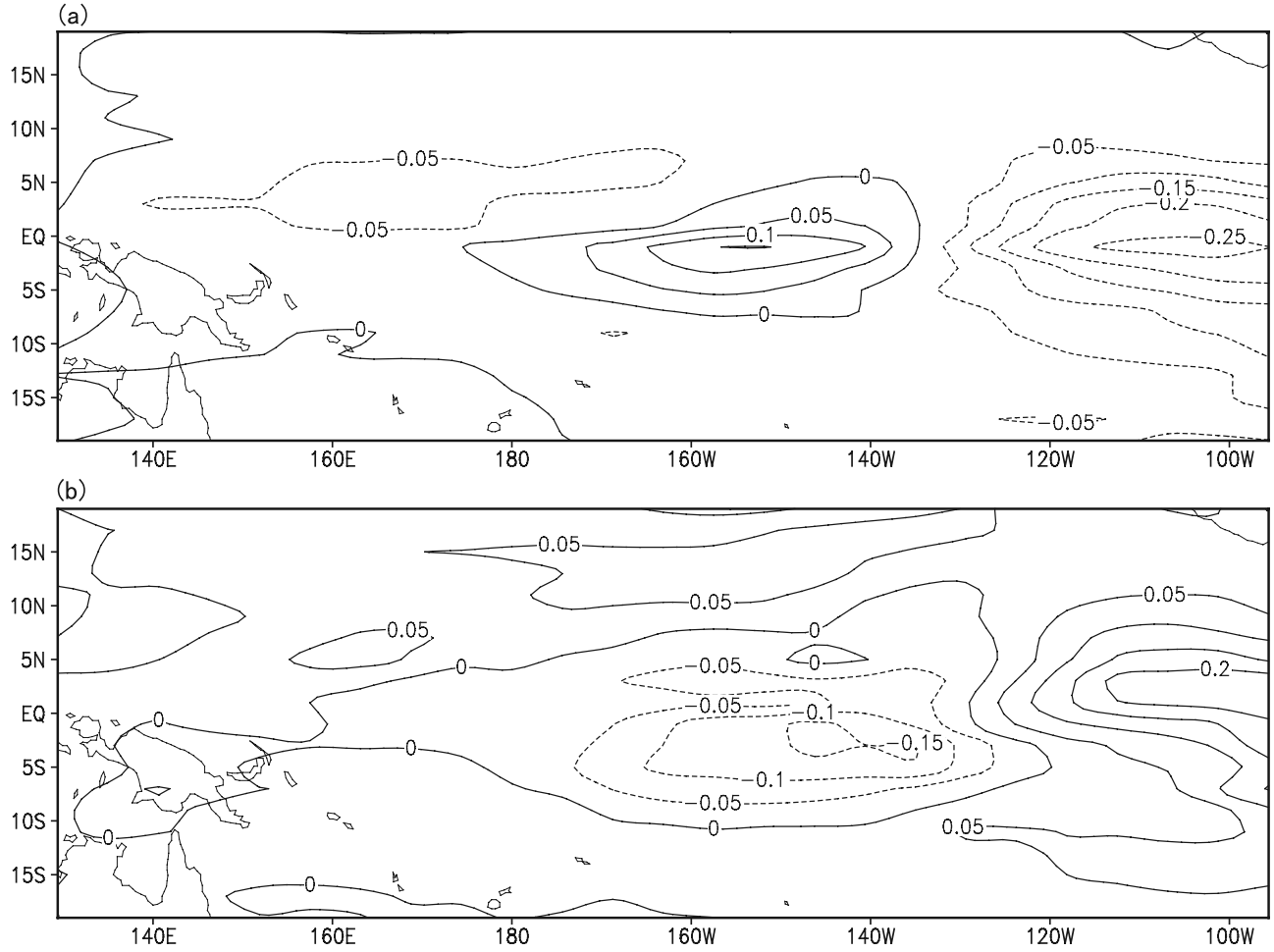

Figure 5. Composite of the initial errors (superimposed on the 40 chosen El Niño events) that exhibit significant season-dependent evolutions: (a) composite of Type I–like errors and (b) composite of Type II–like errors.

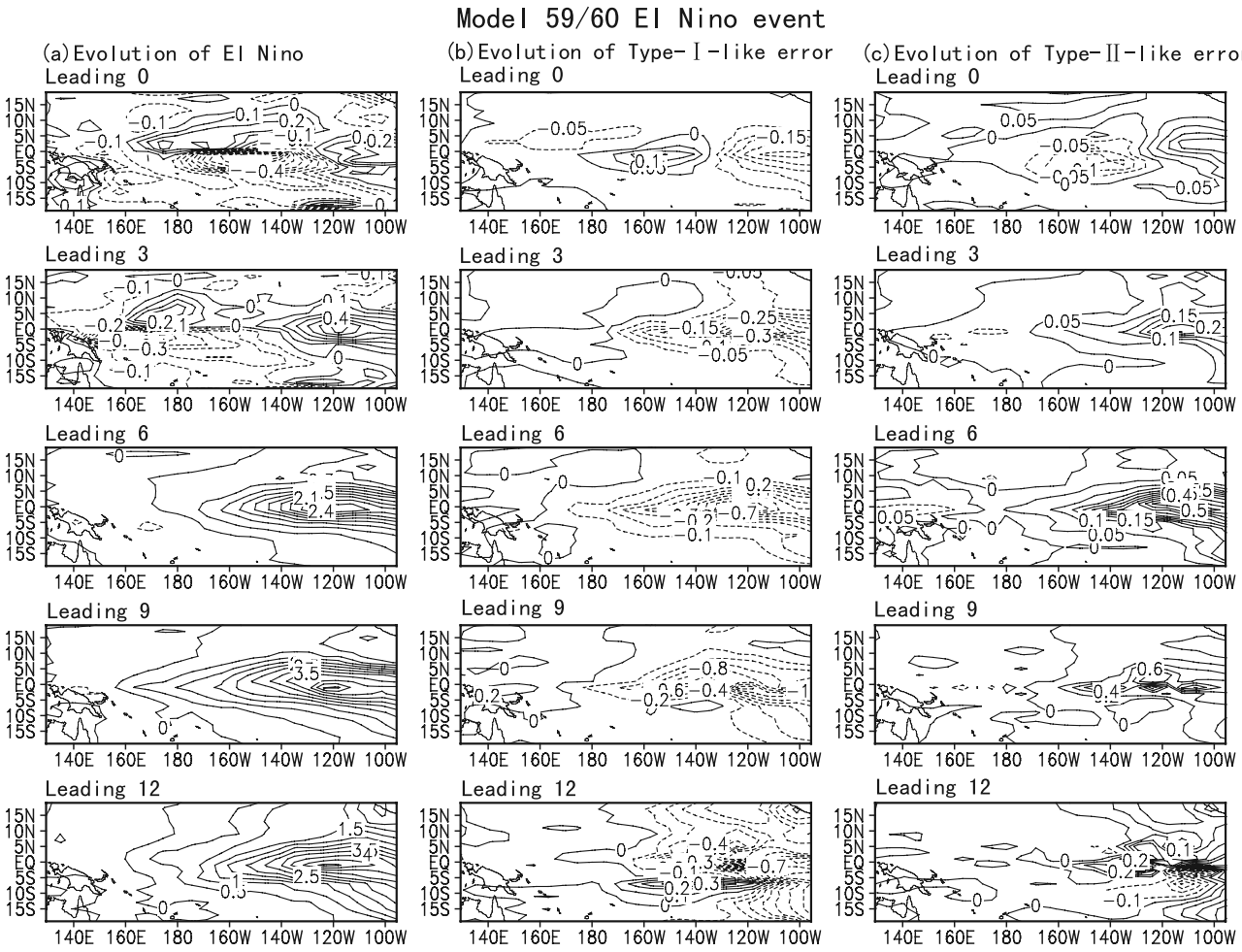

Figure 6. SSTA components for (a) the model 59/60 El Niño event (see Figure 2c) with leading times of 0, 3, 6, 9, and 12 months, (b) the evolutions of the composite Type I–like error shown in Figure 5, and (c) the evolutions of the composite Type II–like error shown in Figure 5.

[28] *Samelson and Tziperman* [2001] applied the approach of a linear singular vector (LSV) in the Zebiak-Cane model to study the SPB for ENSO events, where the LSV is the fastest growth perturbation of the linearized version of the Zebiak-Cane model. They demonstrated that the first empirical orthogonal function (EOF) mode of the LSV of the Zebiak-Cane model has the spatial structure of a mature El Niño event and emphasized that the SPB results from a disturbance growth behavior similar to that of the El Niño event. Our results demonstrate this possibility (for example, Type-II-like errors). Furthermore, we find that the other type of initial errors, which have a growth behavior opposite to that of El Niño events (for example, Type-I-like errors), can also show significant season-dependent evolutions in the Zebiak-Cane model. That is to say, among the initial errors that exhibit season-dependent evolutions related to the SPB for El Niño, some may have the spatial structure of a mature El Niño event, and others may possess that of a mature La Niña event. The latter indicates that the SPB may also result from disturbance growth opposite to that of the El Niño.

[29] In addition, *Xue et al.* [1997] calculated the LSVs of the Zebiak-Cane model and attempted to investigate the initial errors that have the largest effect on El Niño prediction, where the resultant SSTA error patterns have a prominent "seesaw" structure with opposite anomalies between the eastern and western equatorial Pacific. The two types of initial errors shown in this study exhibit features typical of those LSV patterns, such as the zonal dipolar structure of the SSTA component, but the regions associated with the large anomalies are located in the central and eastern equatorial Pacific and tend to be more localized than the LSVs do (compare *Xue et al.* [1997, Figure 17a] and Figure 5 in this paper). This difference could be due to the effect of nonlinearity, which, of course, needs to be studied in depth. Although the two types of error patterns are almost the opposite of each other and imply some linearities, their evolutions (i.e., the resultant prediction errors) show nonlinear effects. To support this argument, we have investigated the evolutions of the two composite initial errors on the 40 El Niño events. For all the strong El Niño events, we took the ensemble mean of the prediction errors (i.e., $E_{Nino\text{-}3}$) caused by the two composite Type-I-like and Type-II-like errors (in Figure 5), respectively. It is shown that the ensemble mean of the NINO3 SSTA prediction errors caused by the composite Type-I-like error is about -0.8635°C, but that caused by the composite Type-II-like

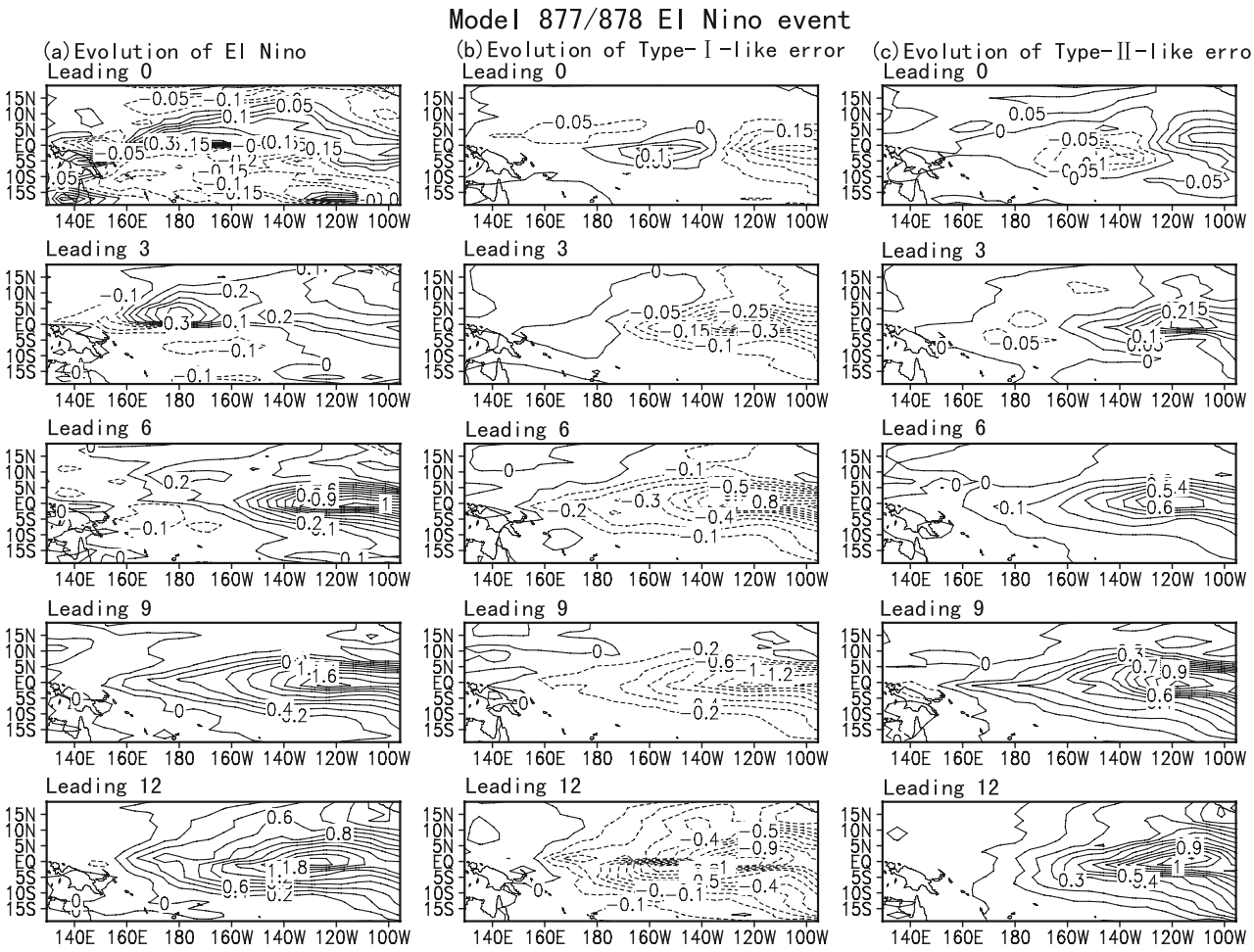

Figure 7. As in Figure 6 but for the model 877/878 El Niño event shown in Figure 2d.

error is 0.3167°C. This amplitude difference exceeds 0.5°C. It is known that two patterns with opposite signs, such as LSVs and -LSVs, will have the same amplitude of evolutions in the linearized model [e.g., *Xue et al.*, 1997; *Mu et al.*, 2007a]. Therefore, we show that the differences between the prediction errors caused by the composite Type-I-like and Type-II-like errors reflect the effect of nonlinearity on the error growth of strong El Niño events. For the weak El Niño events, the amplitude difference between the ensemble means of the NINO3 SSTA prediction errors caused by the composite Types-I-like and Type-II-like errors ia only 0.0812°C and can be neglected. These comparisons indicate that the predictions of strong El Niño events could be affected by relatively strong nonlinearities, while those of weak El Niño events may be affected by weak nonlinearities.

[30] In realistic ENSO predictions, all sorts of initial error patterns may exist because of different initializations and different models. Many studies have been carried out to find the initial error pattern that has the largest effect on the prediction results, for example, the aforementioned *Xue et al.* [1997], *Samelson and Tziperman* [2001], and *Mu et al.* [2007a, 2007b]. The above two types of initial errors may roughly illustrate the error patterns that cause extreme uncertainties in the El Niño prediction through the spring. Furthermore, considering that the regions associated with the large SSTA errors are located in the equatorial east-center Pacific, the Type-I-like and Type-II-like errors may provide some information regarding the "sensitive area" of El Niño predictions. It is conceivable that, if we intensify the observations in the sensitive area rather than in other areas, the ENSO predictions may be greatly improved.

5. Summary and Discussion

[31] The main results of this paper are as follows. Two types of initial errors have been identified to have significant season-dependent evolutions related to the SPB for El Niño events. One type possesses a SSTA component that has a large-scale zonal dipolar pattern with positive anomalies in the central equatorial Pacific and negative anomalies in the eastern equatorial Pacific and tends to cause the El Niño events to be under-predicted through spring; the other type has a zonal dipolar pattern of the SSTA component with negative anomalies in the central equatorial Pacific and positive anomalies in the eastern equatorial Pacific and causes the El Niño events to be over-predicted through the spring. For strong El Niño events, the former error pattern tends to have a larger effect on the prediction than the latter. However, for weak El Niño events, it is very difficult to determine which type of initial errors cause worse prediction. The results also demonstrate that there exist other initial errors that do not induce obvious season-dependent

evolutions; furthermore, a common characteristic cannot be extracted from their patterns. These results suggest that once a particular error mode similar to the two types of initial error patterns has been initiated, the SPB for El Niño events could occur under the model conditions. On the basis of these two types of initial errors, it is also suggested that the initial errors related to the SPB for El Niño events grow in two possible ways: some grow with dynamical behavior similar to that of the El Niño events, and others develop with a tendency opposite to that of the El Niño events. The significant growth of these initial errors during the spring may be also related to the strongest ocean-atmosphere coupling instability occurring in the spring in the climatological annual cycle and the strongest dynamical instability (or the weakest persistence) in the spring of the El Niño events [*Mu et al.*, 2007a]. These two factors, which are determined by models, together with the particular patterns of initial errors, induce the considerable growth of the initial errors during the spring, which essentially results from Bjerknes' positive feedback mechanism.

[32] The two types of initial error patterns are almost opposite to each other and imply some linearities, but the resultant prediction errors show considerable differences for strong El Niño events and reflect the effect of nonlinearity on the prediction uncertainties for El Niño events. The strong (weak) El Niño events have relatively strong (weak) nonlinearities and the corresponding predictions are affected by the relatively strong (weak) nonlinearities.

[33] To reduce the effect of the initial uncertainties on the prediction results, an ensemble forecast technique based on a multiinitial condition ensemble is used in many predictability studies and even many operational forecasts [*Kirtman et al.*, 2002]. In this study, we demonstrate that for a forecast of a single theoretical El Niño event, there exists some perturbed initial conditions that cause the El Niño event to be over-predicted and others that cause the El Niño to be under-predicted. These results imply that if multiple perturbed initial conditions are adopted to predict the El Niño event, the ensemble mean could offer a better forecast as compared to a single forecast. Furthermore, we note that in both two types of initial errors, the regions associated with the large SSTA errors are always located in the equatorial central and eastern Pacific and cause extreme prediction uncertainties. These two types of initial errors may therefore capture the ''sensitive areas'' of ENSO predictions. It is conceivable that if the observations in this area are intensified, ENSO forecasting may be improved.

[34] To investigate the characteristics of initial errors that cause a significant SPB for El Niño events, we chose initial error patterns from a time series of SSTA and thermocline depth anomalies obtained by integrating the model. This strategy may not guarantee that the chosen initial errors cover all realistic error patterns. Thus, the resultant characteristics of initial errors in this paper are only indicative. Although the LSV method aims to find the fastest growing perturbation, it does not consider the effect of nonlinearity, because of its linearity. It is therefore expected that a nonlinear method (for example, the CNOP approach) may provide more useful results. Also, because of the simplicity of the adopted model, the results obtained here may be limited in the model's ability to simulate a real system. Furthermore, since the main characteristics of La Niña events, for example, phase locking, cannot be well modeled by the Zebiak-Cane model [*An and Wang*, 2001], no attempt has been made in this paper to study the corresponding problem for La Niña events.

[35] SPB is an unresolved problem for ENSO predictions and needs to be explored step by step. In this paper, we explored the characteristics of initial errors that cause a significant SPB for El Niño events by performing some perfect model predictability experiments. The model error may also affect the ENSO predictions. In this case, it is unclear whether the characteristics of the initial errors that cause a significant SPB demonstrated in this study would hold in the scenario of imperfect model predictability. To determine this, the effect of the model errors on ENSO predictions should be studied with imperfect model predictability experiments. Furthermore, realistic hindcast experiments should be conducted to apply these theoretical results and examine their reliability. Although these questions are challenge, it is still expected that these questions can be resolved in future work.

[36] **Acknowledgments.** We wish to thank the editor, Raghu Murtugudde, and two anonymous reviewers for their constructive and positive comments. This work was jointly sponsored by the National Nature Scientific Foundation of China (grants 40523001, 40505013, and 40675030) and the National Basic Research Program of China (grants 2006CB403606 and 2007CB411800).

References

An, S.-I., and B. Wang (2001), Mechanisms of locking the El Niño and La Niña mature phases to boreal winter, *J. Clim.*, *14*, 2164–2176.

Bjerknes, J. (1969), Atmospheric teleconnection from equatorial Pacific, *Mon. Weather Rev.*, *97*, 163–172.

Blumenthal, M. B. (1991), Predictability of a coupled atmosphere-ocean model, *J. Clim.*, *4*, 766–784.

Chen, D., S. E. Zebiak, A. J. Busalacchi, and M. A. Cane (1995), An improved procedure for El Niño forecasting, *Science*, *269*, 1699–1702.

Chen, D., M. A. Cane, A. Kaplan, S. E. Zebiak, and D. J. Huang (2004), Predictability of El Niño over the past 148 years, *Nature*, *428*, 733–736.

Jin, E. K., et al. (2008), Current status of ENSO prediction skill in coupled ocean-atmosphere models, *Clim. Dyn.*, *31*, 647–666.

Kirtman, B. P., J. Shukla, M. Balmaseda, N. Graham, C. Penland, Y. Xue, and S. Zebiak (2002), Current status of ENSO forecast skill: A report to the Climate Variability and Predictability (CLIVAR) Numerical Experimentation Group (NEG), CLIVAR Working Group on Seasonal to Interannu. Predict., Clim. Variability and Predictability, Southampton Oceanogr. Cent., Southampton, U. K.

Latif, M., T. P. Barnett, M. A. Cane, M. Flugel, N. E. Graham, H. von Storch, J. S. Xu, and S. E. Zebiak (1994), A review of ENSO prediction studies, *Clim. Dyn.*, *9*, 167–179.

Lau, K.-M., and S. Yang (1996), The Asian monsoon and predictability of the tropical ocean-atmosphere system, *Q. J. R. Meteorol. Soc.*, *122*, 945–957.

Lorenz, E. N. (1975), Climate predictability, in *The Physical Basis of Climate Modelling*, *Global Atmos. Res. Programme Publ. Ser.*, vol. 16, pp. 132–136, World Meteorol. Org., Geneva.

McPhaden, M. J. (2003), Tropical Pacific Ocean heat content variations and ENSO persistence barriers, *Geophys. Res. Lett.*, *30*(9), 1480, doi:10.1029/2003GL016872.

Moore, A. M., and R. Kleeman (1996), The dynamics of error growth and predictability in a coupled model of ENSO, *Q. J. R. Meteorol. Soc.*, *122*, 1405–1446.

Mu, M., W. S. Duan, and B. Wang (2003), Conditional nonlinear optimal perturbation and its applications, *Nonlinear Process. Geophys.*, *10*, 493–501.

Mu, M., W. S. Duan, and B. Wang (2007a), Season-dependent dynamics of nonlinear optimal error growth and El Niño–Southern Oscillation predictability in a theoretical model, *J. Geophys. Res.*, *112*, D10113, doi:10.1029/2005JD006981.

Mu, M., H. Xu, and W. Duan (2007b), A kind of initial errors related to ''spring predictability barrier'' for El Niño events in Zebiak-Cane model, *Geophys. Res. Lett.*, *34*, L03709, doi:10.1029/2006GL027412.

Pan, A., Q. Liu, and Z. Liu (2005), Periodic forcing and ENSO suppression in the Cane-Zebiak model, *J. Oceanogr.*, *61*, 109–113.

Samelson, R. G., and E. Tziperman (2001), Instability of the chaotic ENSO: The growth-phase predictability barrier, *J. Atmos. Sci.*, *58*, 3613–3625.

Smith, L. A., C. Ziehmann, and K. Fraedrich (1999), Uncertainty dynamics and predictability in chaotic systems, *Q. J. R. Meteorol. Soc.*, *125*, 2855–2886.

Tang, Y., Z. Deng, X. Zhou, Y. Cheng, and D. Chen (2008), Interdecadal variation of ENSO predictability in multiple models, *J. Clim.*, *21*, 4811–4833.

van Oldenborgh, G. J., M. A. Balmaseda, L. Ferranti, T. N. Stockdale, and D. L. T. Anderson (2005), Evaluation of atmospheric fields from the ECMWF seasonal forecasts over a 15-year period, *J. Clim.*, *18*, 3250–3269.

Walker, G. T. (1924), Correlation in seasonal variations of weather IX: A further study of world weather, *Mem. Indian Meteorol. Dep.*, *24*, 275–332.

Wang, B., and Z. Fang (1996), Chaotic oscillation of tropical climate: A dynamic system theory for ENSO, *J. Atmos. Sci.*, *53*, 2786–2802.

Wang, C., and J. Picaut (2004), Understanding ENSO physics: A review, in *Earth's Climate: The Ocean-Atmosphere Interaction*, *Geophys. Monogr. Ser.*, vol. 147, edited by C. Wang, S.-P. Xie, and J. A. Carton, pp. 21–48, AGU, Washington, D. C.

Webster, P. J. (1995), The annual cycle and the predictability of the tropical coupled ocean-atmosphere system, *Meteorol. Atmos. Phys.*, *56*, 33–55.

Webster, P. J., and S. Yang (1992), Monsoon and ENSO: Selectively interactive systems, *Q. J. R. Meteorol. Soc.*, *118*, 877–926.

Xu, H., and W. S. Duan (2008), What kind of initial errors cause the severest prediction uncertainty of El Niño in Zebiak-Cane model, *Adv. Atmos. Sci.*, *25*, 577–584.

Xue, Y., M. A. Cane, S. E. Zebiak, and M. B. Blumenthal (1994), On the prediction of ENSO, a study with a low-order Markov model, *Tellus, Ser. A*, *46*, 512–528.

Xue, Y., M. A. Cane, and S. E. Zebaik (1997), Predictability of a coupled model of ENSO using singular vector analysis. Part II: Optimal growth and forecast skill, *Mon. Weather Rev.*, *125*, 2043–2056.

Zebiak, S. E. (1986), Atmospheric convergence feedback in a simple model for El Niño, *Mon. Weather Rev.*, *114*, 1263–1271.

Zebiak, S. E., and A. Cane (1987), A model El Niño–Southern Oscillation, *Mon. Weather Rev.*, *115*, 2262–2278.

W. Duan and M. Mu, LASG, Institute of Atmospheric Physics, Chinese Academy of Sciences, Beijing 100029, China. (duanws@lasg.iap.ac.cn)

X. Liu and K. Zhu, Department of Atmospheric Science, Chengdu University of Information Technology, Chengdu 610225, China.